Article

Functionally Graded Piezoelectric Energy Harvester: A Numerical Study

Anuruddh Kumar [1,*], Mohamed Nainar Mohamed Ansari [2,*], Sobhy M. Ibrahim [3], Paramanandam Thomas [4] and Rahul Vaish [5]

1   Hanyang Institute of Technology (HIT), Hanyang University, Seoul 133-791, Korea
2   Institute of Power Engineering, Universiti Tenaga Nasional, Kajang 43000, Selangor, Malaysia
3   Department of Biochemistry, College of Science, King Saud University, P.O. Box 2455, Riyadh 11451, Saudi Arabia
4   Central Power Research Institute, Dielectric Materials Division, Bengaluru 560080, India
5   School of Engineering, Indian Institute of Technology Mandi, Suran 175005, India
*   Correspondence: anuruddh07@hanyang.ac.kr (A.K.); ansari@uniten.edu.my (M.N.M.A.)

Abstract: The performance of linear energy harvesters is primarily confined to a very narrow operating frequency bandwidth around its natural frequency. Even a slight deviation of the excitation frequency from the fundamental frequency of the system tremendously reduces the harvester's performance. In order to minimize this shortcoming, the presented study considers the piezoelectric energy harvester with magnets introducing non-linearity in the system. The simple harmonic balance method is used to solve the non-linearity and for computing the voltage output and power in the frequency domain. In addition, the study also incorporates the functionally graded piezoelectric materials because of their superior properties. The distance between magnets (d_0) has been varied from 0.4 mm to 10 mm along with grading index (n) in the range of 0 to ∞. Finally, voltage and power across the resistance were computed. The effective harvesting frequency range for $d_0 = 0.4$ mm and $n = 1$ is observed in the range of 20 Hz to 85 Hz, while it was only between 35 Hz and 65 Hz for $d_0 = 10$ mm, yielding a 216% increase in the frequency bandwidth. Under different case studies, the peak output power varied from 2 mW ($d_0 = 0.4$ mm and $n = ∞$) to 6 mW ($d_0 = 10$ mm and $n = 0$).

Keywords: functionally graded piezoelectric material (FGPM); energy harvesting; nonlinear vibration

1. Introduction

During the last few decades, linear and nonlinear energy harvesters have been a point of interest for the researchers and scientists for converting waste vibration energy into electrical energy [1–4]. In the most recent decade, a lot of improvement happened in nanotechnology which also affect the very-large-scale integration (VLSI) technology. Nanosensors devices or systems are being developed for various applications, most notably in healthcare and medical industries, military defense and environmental and agricultural industries. These systems can drive with very low power consumption. For this purpose, batteries are required to drive this type of device, which comes with a lot of drawbacks also. Batteries limit the size of Nanosensors devices or systems. Sometimes, the replacement of a battery can be costly, such as in peacemaker applications. However, there are a lot of energy sources, such as solar, thermal, vibration, or radiofrequency, liable to the working environment of the system. Apart from solar energy harvesting, energy extraction from vibration has gained much more attention from researchers, as it is widely available in the environment. Electromagnetic and piezoelectric technology are popular to extract energy for vibrating systems. Electromagnetic technology has a lot of drawbacks when scaling down in size due to increments in losses. For micro-electro-mechanical Systems (MEMS), piezoelectric energy harvesting technology provides more potential, as it is easy to integrate and highly sensitive to vibration.

Although, the concept of nonlinearity demands a complex understanding, it is advantageous in comparison with the linear harvester in terms of the bandwidth of excitation frequency. In the case of linear harvesters, the power reduces drastically if the excitation frequency is slightly away from its natural frequency [5]; in contrast, with nonlinearity in the harvester, the effective harvesting frequency bandwidth can be increased significantly.

Researchers have explored various mechanisms to introduce the nonlinear dynamic phenomenon in energy harvesting applications. Mann and Sims [6] used magnetic restoring force to levitate an oscillating center magnet for electromagnetic energy harvesting. Harmonic base excitation has been considered as input energy to study the resulting Duffing's equation. R. Ramlan et al. [7] studied nonlinear energy harvesters with two types of non-linear stiffnesses: the first system considered a non-linear bistable snap-through mechanism, while in the second system, nonlinearity is invoked with the hardening of the spring. Daqaq [8] theoretically investigated the monostable Duffing's oscillator for colored excitations and Gaussian white noise. The authors also studied other types of nonlinearities such as damping and inertial nonlinearities, capable of enhancing the performance of the harvester's operation. Stanton C. et al. [9] investigated the hardening and softening response of piezoelectric energy harvesters, which were invoked by the tuning of magnetic interaction. The study concludes that a nonlinear energy harvester is suitable for ambient excitation with slow varying frequencies. Kang-Qi Fan [10] proposed a design and experimental verification of a compact bi-directional nonlinear energy harvester. The proposed design has two magnetically coupled piezoelectric cantilever beams with orthogonal directions of deflection. Experimental verifications spotlighted the advantages of a nonlinear piezoelectric energy harvester over the linear ones.

On the other side, scientists and researchers explored advanced manufacturing technologies to improve the mechanical performance or control numerous properties in a desirable direction. These materials are called functionally graded materials (FGMs), in which properties are controlled in the volume using grading index (n) [11–14]. The merit of using these materials is that the mechanical properties can be controlled at the layer interface and make smooth stress variation at the interface of the ceramic layer (piezoelectric) and metal layer to avoid debonding at the interface [15,16].

Theoretical and, up to some extent, experimental studies of the functionally graded materials have been reported in the literature for energy harvesting and active control system applications [17–20]. However, FGMs' performance was not explored for cantilever-based nonlinear harvesters. In this paper we report the performance of the functionally graded piezoelectric nonlinear energy harvester and compare it with the linear functionally graded piezoelectric energy harvester. It is to note that FGMs are difficult to prepare. Most of the studies are reported with FGMs, which are almost difficult to fabricate. On the other hand, authors have considered FGM, which has already been experimentally fabricated by some other group. Hence, the present study is closer to actual performance. Dynamic studies have been carried out in time and frequency domains. However, a frequency domain has limited use for nonlinear systems (only for excitations with one frequency and one harmonic function), as the superposition principle is not valid anymore. For other types of excitation, e.g., random excitation, some linearization techniques may be required.

2. Formulation of Functionally Graded Piezoelectric Material Nonlinear Energy Harvester

The schematic of the functionally graded piezoelectric material nonlinear energy harvester is shown in Figure 1. In this harvester, two piezoelectric layers are attached to the host structure to form the sandwich structure. These piezoelectric layers are connected in parallel with an external load resistor (R). The host layer is made of aluminum, while the piezoelectric layer is assumed to be made of functionally graded piezoelectric materials. For introducing the nonlinearity, one magnet is attached at the free end of the cantilever and another magnet is placed in front of the first magnet. Grading is done according to

power law distribution in terms of volume fraction. Material properties for the functionally graded piezoelectric material can be given as [21],

$$P_{eff}^{PT}(z) = \left(P_T^{PT} - P_B^{PT}\right)\left(\frac{2z - h_s}{2h_{PT}}\right)^{n_2} + P_B^{PT} \qquad \frac{h_s}{2} \leq z \leq \frac{h_s}{2} + h_p \tag{1}$$

$$P_{eff}^{PB}(z) = \left(P_T^{PT} - P_B^{PT}\right)\left(1 + \frac{2z + h_s}{2h_{PB}}\right)^{n_3} + P_B^{PB} \qquad -\frac{h_s}{2} - h_p \leq z \leq -\frac{h_s}{2}$$

where, P_T and P_B are material properties of top and bottom surface of the layer. h_P is thicknesse of the top and bottom piezoelectric layers. h_s is the thickness of the host layer. Superscript s, T and B represent the host layer, top piezoelectric and bottom piezoelectric layers.
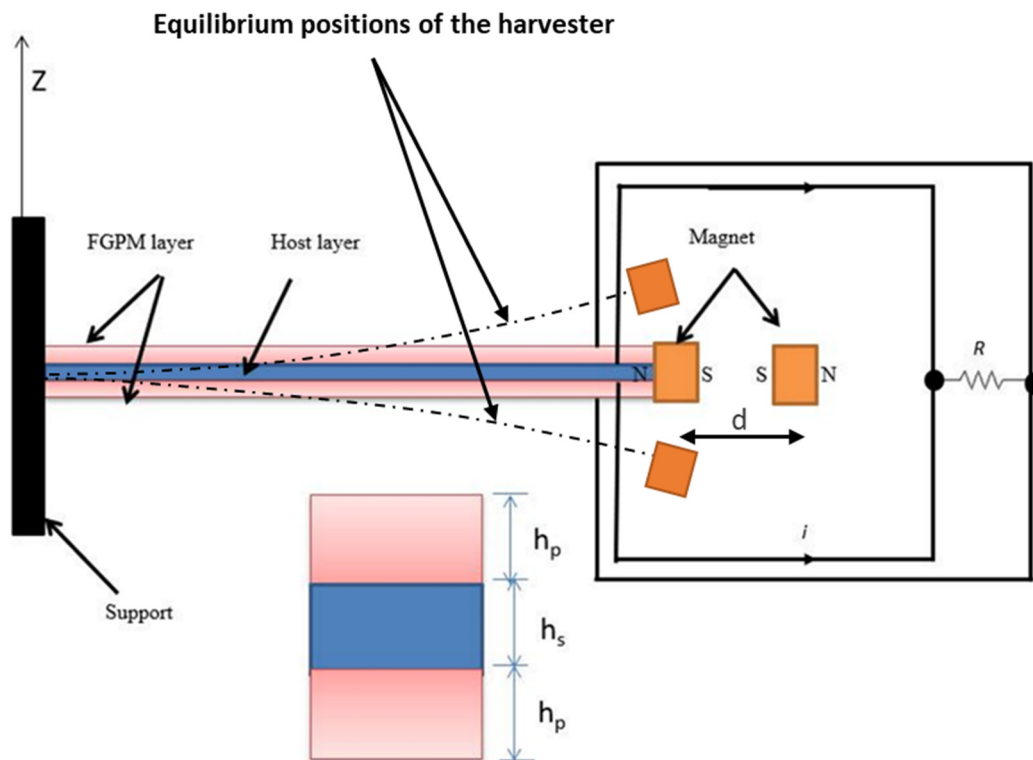

Figure 1. Schematic of the functionally graded piezoelectric material nonlinear energy harvester.

2.1. Modeling of the Magnetic Force:

Figure 2 shows a simplified representation of the magnetic force on the proof mass. As bimorph is stiff along the length of the cantilever, the magnetic force component (F_{magh}) in the longitudinal direction of the cantilever is assumed negligible. The vertical component of the repulsive force (F_{magv}) between the opposite poles of the magnet is evaluated using Taylor series expansion [22,23],

$$F_{magv} \cong \frac{F_{mag}z}{d_0} - \frac{F_{mag}z^3}{2d_0^3}$$
$$where \tag{2}$$
$$\frac{F_{mag}}{d_0} = K_1 \quad and \quad \frac{F_{mag}}{2d_0^3} = K_3$$

where, F_{mag} is the repulsion force. K_1 and K_3 are parameters occurring due to the linear and cubic component of the magnetic force (F_{mag}). Validation of the magnetic force against literature is shown in Figure 3, which shows a good agreement with the current modeling of the magnetic force.
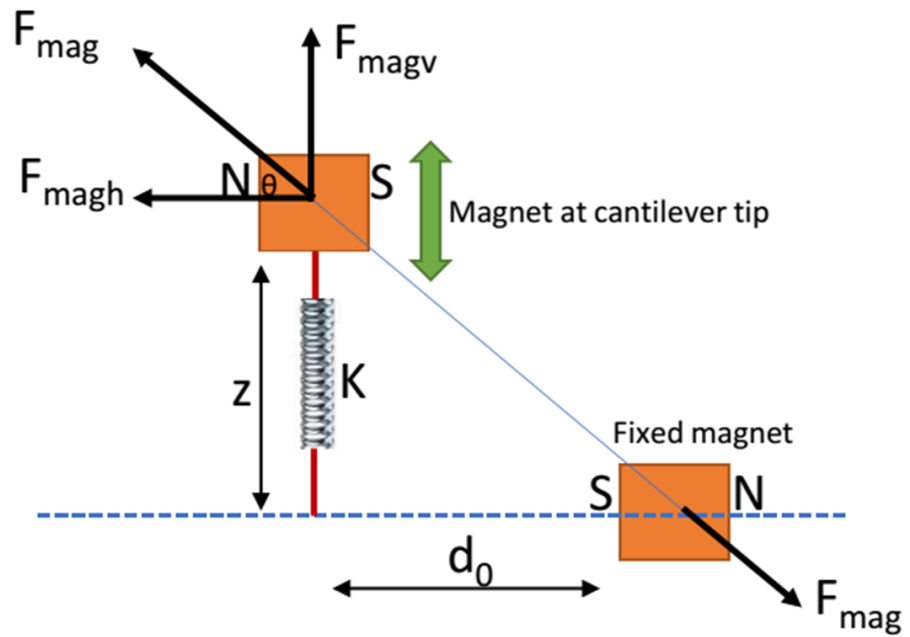
Figure 2. Modeling of the magnetic force for a cantilever energy harvester.
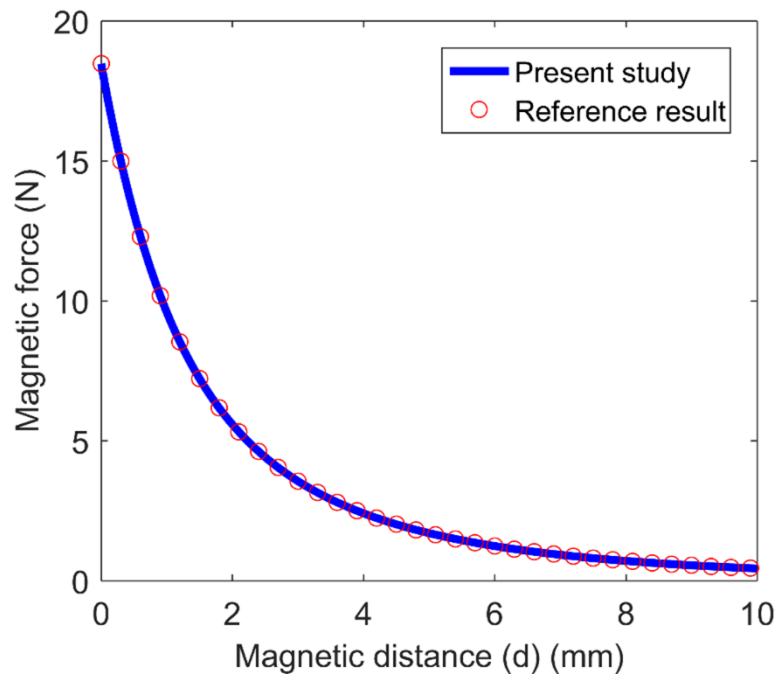

Figure 3. Validation of magnetic force between two magnets with reference (Al-Ashtari et al., 2012) results.

2.2. Finite Element Formulation

For the finite element formulation, plate elements have been considered with five degrees of freedom (3 translations, 2 rotations) per node. One additional degree of freedom (voltage) has been considered for piezoelectric layers. The linear piezoelectric constitutive equations are given as

$$\{D\} = [e]\{\varepsilon\} + [b]\{E\}$$
$$\{\sigma\} = [Q]\{\varepsilon\} - [e]^T\{E\} \tag{3}$$

where $\{D\}$, $\{\sigma\}$, $[Q]$, $[e]$ and $[b]$ represent electric displacement, stress, elastic stiffness coefficients, piezoelectric stress coefficient and dielectric constant matrices, respectively.

Using Hamilton's principle, the governing equations for the harvester can be written as [23],

$$[M]\{\ddot{q}\} + [C]\{\dot{q}\} + [K_{uu} - K_1]\{q\} + [K_3]\{q\}^3 + [K_{u\phi}]\{\phi_p\} = \{F_m\}$$
$$[K_{\phi u}]\{\dot{q}\} + [K_{\phi\phi}]\{\dot{\phi}_p\} + \frac{\phi_p}{R} = 0 \tag{4}$$

where $[M]$, $[C]$ and $[K_{uu}]$ are the mass matrix, damping matrix and stiffness matrix, respectively. $[K_1]$ and $[K_3]$ are the elemental stiffness matrices due to the linear and cubic components of the magnetic force, respectively. $[K_{u\phi}]$ and $[K_{\phi\phi}]$ are the piezoelectric coupling matrix and elemental capacitance matrix, respectively. $\{F_m\}$ is the external base excitation force. $\{q\}$ is the displacement matrix, and $\{\phi_p\}$ is the voltage across the layers. R is the resistance across the piezoelectric layers.

Using modal analysis, the equations for the fundamental vibration mode of the harvester can be given as

$$m\ddot{r} + c\dot{r} + kr + k_m r^3 + \theta_p \phi = F_{m_{eq}}$$
$$\theta_p \dot{r} + c_p \dot{\phi} + \frac{\phi}{R} = 0 \tag{5}$$

where 'r' is the amplitude of the corresponding mode of the displacement expressed by generalized coordinates (z); θ_p is the piezoelectric coupling coefficient, and C_p is the capacitance of the piezoelectric layers. k_m is the generalized stiffness coefficient accounting for the magnetic force within the system.

The electric power (P) across the load resistance can be written as [24].

$$P = \frac{\phi^2}{R} \tag{6}$$

2.3. Harmonic Balance Method

Simulation of the equation of motion, Equation (5), can be carried out straightforwardly in a time domain. However, in this case of the energy harvester, the solution in the frequency domain is most desirable, as it contains information for different frequency excitations. An excitation with multiple frequencies is not covered, as the superposition principle cannot be employed for nonlinear systems. In literature, different methods are proposed to calculate the response of nonlinear vibration in frequency domain, such as the method of harmonic balance, the averaging method and the method of multiple scales. Harmonic balance method has been extensively employed to study Duffing's oscillators and nonlinear energy harvesters [25–27]. This method provides the response of the harvester for a wide range of frequency excitations. In this method the solution of the harvester is presumed to have different combinations of harmonic terms. In the present study, we assume the excitation force to be $F\cos(\omega t)$. To obtain an approximate solution for r and ϕ (Equation (5)), a first order expansion using one frequency is considered that can be written as

$$r = a_0 + a_1 \sin(\omega t) + b_1 \cos(\omega t)$$
$$\phi = c_1 \sin(\omega t) + d_1 \cos(\omega t) \tag{7}$$

Substituting Equation (7) into Equation (5), the following equations can be obtained.

$$m(-a_1\omega^2 \sin(\omega t) - b_1\omega^2 \cos(\omega t)) + c(a_1\omega \cos(\omega t) - b_1\omega \sin(\omega t)) + k(a_0 + a_1 \sin(\omega t)$$
$$+b_1\cos(\omega t)) + k_m(a_0 + a_1\sin(\omega t) + b_1\cos(\omega t))^3 - \theta_p(c_1\sin(\omega t) + d_1\cos(\omega t)) = F\cos(\omega t) \tag{8}$$

$$\theta_p(a_1\omega \cos(\omega t) - b_1\omega \sin(\omega t)) + c_p(c_1\omega \cos(\omega t) - d_1\omega \sin(\omega t))$$
$$+(c_1 \sin(\omega t) + d_1 \cos(\omega t))/R = 0 \tag{9}$$

Due to the harmonic balance method, only the constant term and the components of $\sin(\omega t)$ and $\cos(\omega t)$ are balanced.

Comparison of the constant terms of both sides of Equation (8) leads to

$$-\left(\frac{1}{4}\right)k_m\left(-4a_0^3 - 6a_0a_1^2 - 6a_0b_1^2\right) + a_0k = 0 \tag{10}$$

Similarly, by comparing the coefficients of $\cos(\omega t)$ and $\sin(\omega t)$ on both sides of Equation (8), the corresponding condition can be written as

$$-b_1m\omega^2 + a_1c\omega + b_1k - (1/4)\alpha(-12a_0^2b_1 - 3a_1^2b_1 - 3b_1^3) - \theta_pd_1 = F \tag{11}$$

$$-a_1m\omega^2 - b_1c\omega + a_1k - \left(\frac{1}{4}\right)k_m\left(-12a_0^2a_1 - 3a_1^3 - 3a_1b_1^2\right) - \theta_pc_1 = 0 \tag{12}$$

By making similar comparison for the coefficients of $\cos(\omega t)$ and $\sin(\omega t)$ from Equation (9), we obtain following equations:

$$c_pRc_1\omega + Ra_1\omega\theta_p + d_1 = 0 \tag{13}$$

$$-c_pRd_1\omega - Rb_1\omega\theta_p + c_1 = 0 \tag{14}$$

c_1 and d_1 can be expressed in terms of a_1 and b_1.

$$c_1 = (-c_pR^2a_1\omega^2\theta_p + Rb_1\omega\theta_p)/(c_p^2R^2\omega^2 + 1) \tag{15}$$

$$d_1 = (-c_pR^2b_1\omega^2\theta_p - Ra_1\omega\theta_p)/(c_p^2R^2\omega^2 + 1) \tag{16}$$

Equations (15) and (16) will be used in Equations (10)–(12) to solve for a_0, a_1 and b_1. However, if the vibration is confined to an interwell oscillation, then the constant term in the assumed solution of r can be considered to be zero ($a_0 = 0$) [26].

After knowing the values of a_0, a_1 and b_1, electrical parameters c_1 and d_1 can be easily calculated by solving Equations (15) and (16).

3. Validation Studies

The current formulation is divided into several parts and validated at different steps. First, the validation in terms of variation of magnetic force with distance between two magnets is performed; afterwards, the output open circuit voltage for different frequencies and finally the simple harmonic balance method is validated by using a velocity-displacement diagram.

3.1. Validation of Magnetic Force

Since the non-linear energy harvester has been modelled using Duffing's equation by using magnets, it becomes mandatory to validate the variation of the magnetic force with distance. In the present study, the magnetic force is defined as a function of separation distance between the two magnets and their properties. Here, for the validation purpose, only two magnets of 10 mm × 4.5 mm × 4.5 mm with a residual flux density of $B_r = 1.48$ T have been considered. We have recovered the variation of the magnetic force provided by Ashtari et al. [28] completely as presented in Figure 3 and summarize it in tabular form in Table 1.

Table 1. Validation of magnetic force with reference results.

Distance (mm)	Magnetic Force (N) (Reference)	Magnetic Force (N) (Present)
0	18.47	18.44
3	3.558	3.555
6	1.239	1.234
9	0.552	0.540
10	0.4473	0.4471

3.2. Validation of Open Circuit Voltage from Harvester

In order to validate the piezoelectric formulation developed, we have conducted experiments. For the validation purpose, we have taken a beam with a piezoelectric patch made of PZT-5A, as shown in Figure 4. Geometrical parameters are given in Table 2. It is to be noted that for experimental validation, only a part of the beam is covered with piezoelectric patches and not the whole length as shown in Figure 1. With the help of a vibration generator (Philip Harris-B8H30701), the harvester is excited with a fixed amplitude (10 mm) and varying excited frequency range (3.5 Hz to 20 Hz) conditions at the fixed end of the cantilever. The variation of the open circuit voltage with frequency (Figure 5) obtained from the numerical simulation is found to be in a good agreement with the experimental results, concluding that the formulation of all the matrices presented in Equation (5) is correct.
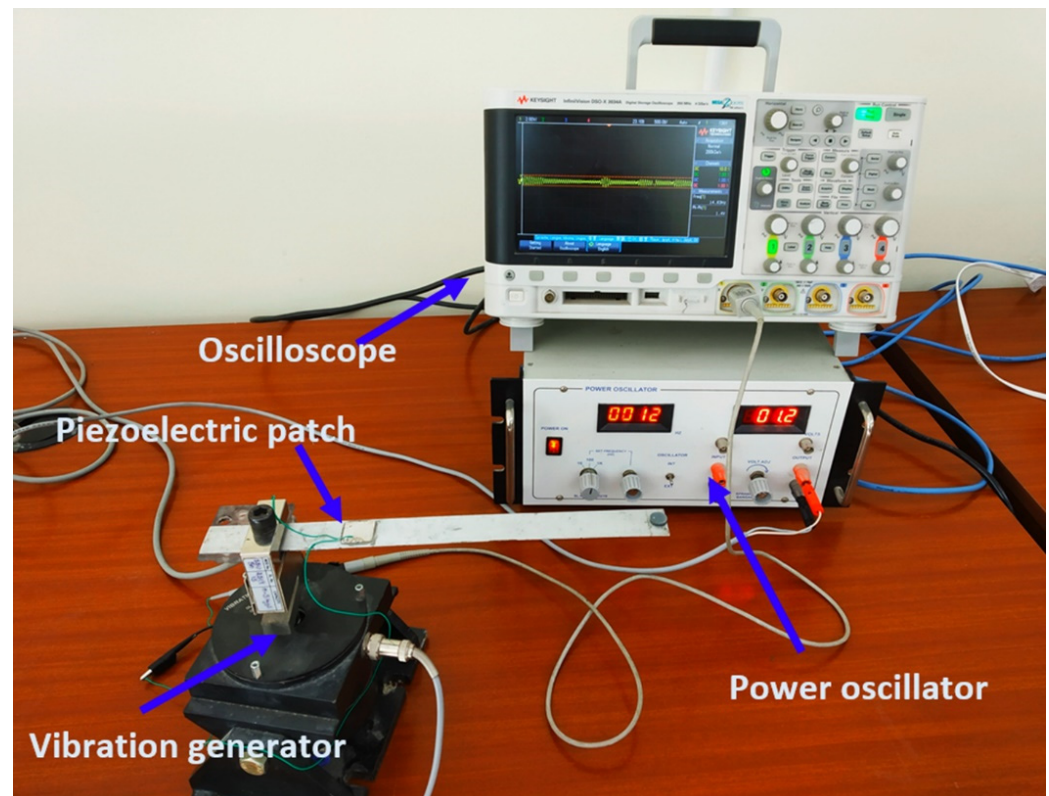

Figure 4. Experimental setup for piezoelectric cantilever beam.

Table 2. Geometrical parameters of cantilever in experimental setup.

Geometrical Parameters	Value
Length of the cantilever beam	250 mm
Width of beam	25 mm
Thickness of beam	0.5 mm
Length of Piezoelectric patch	20 mm
Width of piezoelectric patch	20 mm
Thickness of the piezoelectric layer	0.5 mm
Distance of piezoelectric patch from fixed end	50 mm
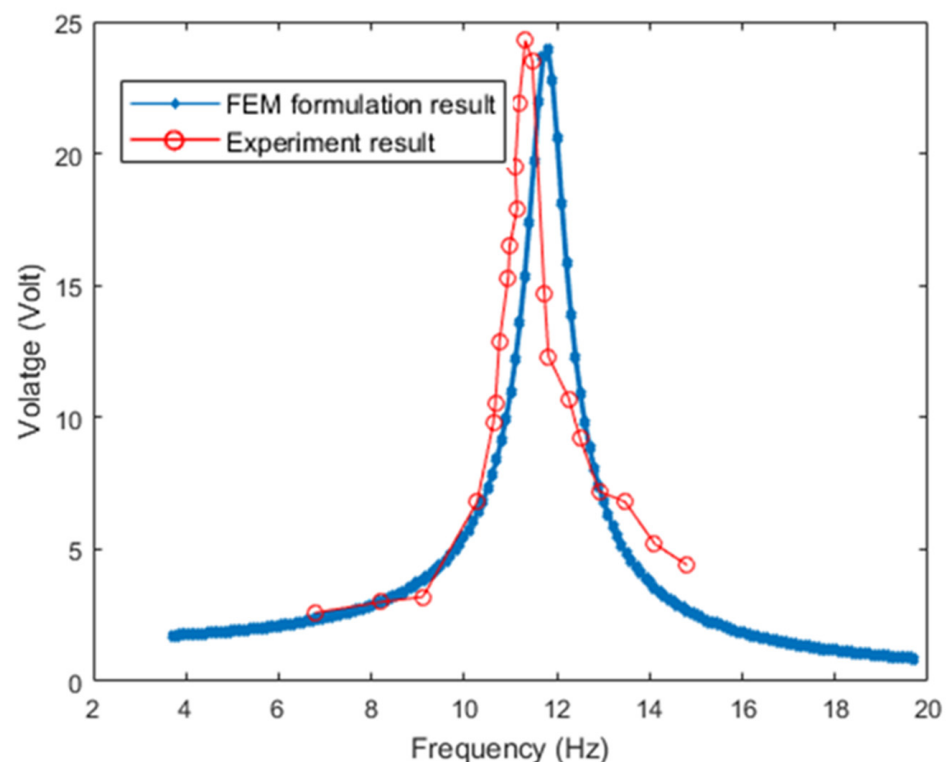
Figure 5. Validation of FEM formulation with experiment for the piezoelectric cantilever beam.

3.3. Validation of Simple Harmonic Balance Method

The present formulation of the simple harmonic balance method is validated with the solution provided by Marathe et al. [29] with certain modifications. For the validation, the initial excitation was given to the system, and the velocity vs. displacement diagram (as presented in Figure 6) is plotted against the reference results. In view of above validations, it can be concluded that Equation (5) has been solved appropriately using the simple harmonic balance method.
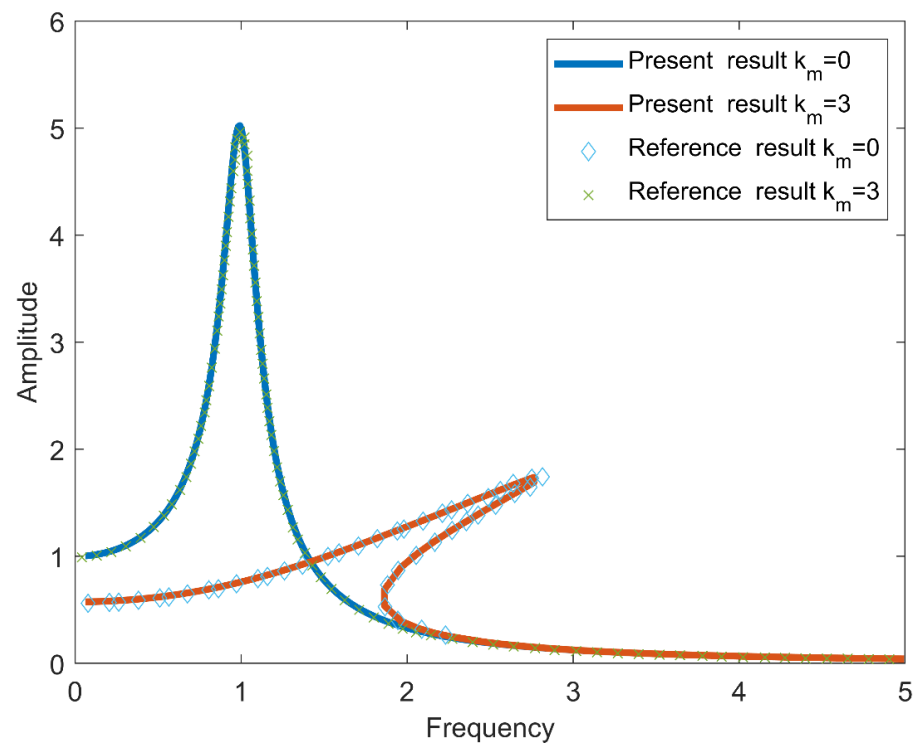
Figure 6. Validation of simple harmonic balance method with reference [29] results.

4. Numerical Studies

To study the functionally graded piezoelectric material energy harvester, a cantilever structure has been adopted. To introduce the nonlinearity in the structure, one magnet is used at the free end of the cantilever and another at a distance d_0, as shown in Figure 1. Magnets are placed such that there are repulsive forces between the two magnets. Due to the repulsive force, the position of the magnet is stable at two extreme points along the direction of vibration. The force between the magnets can be altered by changing the distance between them. To support the piezoelectric materials, aluminum is used for the host layer. PZT-Pt (Pb(Zr,Ti)O$_3$-Pt) was selected as FGM for numerical studies. Takagi et al. [16] attempted a fabrication of the above mentioned FGM and have reported physical properties up to PZT-30%Pt. In this study, the top surface of the upper piezoelectric layer is considered as PZT-0%Pt, while PZT-20%Pt is considered for the bottom surface. Similarly, the top surface of the lower piezoelectric layer is made of PZT-20%Pt and PZT-0%Pt for the bottom surface. The grading index (n) controls the distribution of piezoelectric properties in the thickness direction of the piezoelectric layers according to Equation (1). Geometrical and material properties are listed in Tables 3 and 4, respectively. For these material properties, variations of Young's modulus for different grading indexes has been shown in Figure 7. For grading index $n = 0$, there is a ductile–brittle interface between the host layer (ductile) and piezoelectric material (brittle), which is prone to debonding failure. However, as grading index (n) increases, the ductility increases at the interface due to addition of the PZT-20%Pt material. At grading index $n = 1000$, the piezoelectric material has more ductility, which enhances the interface bonding but reduces its piezoelectric properties.

Table 3. Geometrical properties of the functionally graded piezoelectric energy harvester.

Geometrical Parameters	Value
Length of the cantilever beam	150 mm
Width of beam	6 mm
Thickness of host layer	1 mm
Thickness of the piezoelectric layer	0.5 mm

Table 4. List of materials properties [16].

Material Properties	PZT-0% Pt	PZT-20% Pt	Aluminum
Young's modulus, Y (GPa)	63	84.8	70
Density, ρ (kg/m^3)	7500	10,290	2707
Poisson's ratio, υ	0.3	0.342	0.3
Piezoelectric constant, d_{31} (pC/N)	-164	-98	Conductive layer
Dielectric constant (at constant stress), $\varepsilon_{33}/\varepsilon_{o}$	1653	2927	Conductive layer

To verify the advantage of the functionally graded piezoelectric material, a static study has been carried out for a linear harvester. A point force is applied at the tip of the cantilever to induce bending of the cantilever, which generates stresses in the cantilever along the length. Figure 8a shows the variation of the stress (σ_x) in the thickness direction of the harvester for different grading indexes (n). For this study, n is varying from $n = 0$ to $n \rightarrow \infty$, where $n = 1000$ has been considered as $n \rightarrow \infty$. From Equation (1), it is easy to calculate the variation of PZT-0%Pt to PZT-20%Pt in the piezoelectric layer in thickness direction. In the cantilever, the piezoelectric layers are completely made from PZT-0%Pt for $n = 0$ and PZT-20%Pt for $n = 1000$. Hence, the proportion of PZT-20%PT increases with the value of the grading index. From Figure 8, it can be concluded that the grading index has an impact on the stress distribution in the thickness direction. Stress variations at the layer interface become smoother with an increase in grading index. If the piezoelectric layer has grading index zero ($n = 0$), then stress variation increases at the interface of the layers between the host layer and piezoelectric layer due to 100% piezoelectric (PZT-0%Pt) and 100% metal (Aluminum) bonding. It is to be noted that in Figure 8, a sharp bend in the stress variation curve for $n = 0$ is observed inside the host structure. This is due to the fact that in finite element formulation, we calculate stress values at Gauss integration points, which lie inside the thickness of a particular layer. A similar conclusion can be drawn from Figure 8b, which shows the strain energy variation in thickness direction. There is a smooth strain energy variation in the cantilever along the thickness.

After performing the static analysis, simulations for a dynamic study have been performed for the energy harvester. The base of the harvester is accelerated sinusoidally with an amplitude of 1 g and varying frequency in the range of 20 Hz to 100 Hz. In this study, mechanical damping (0.2%) considered as mechanical loss during harmonic force. The linear harvester is only effective when the excitation frequency is close to its natural frequency (52 Hz) with any magnetic force. The power drastically decreases as the excitation frequency is away from the resonance frequency. Here, a wider frequency range is chosen due the unpredictable nature of the ambient vibrations. Simulations are performed for different energy harvesters which are having different grading indices (n) in the piezoelectric layer as well as different distances between the magnets varying from 0.4 mm to 1 mm. Due to the magnetic force, nonlinearity is introduced in the energy harvester. The magnitude of the magnetic force can be altered with the help of the distance between the magnets. The energy harvester has more than one equilibrium if the force is applied beyond a certain load. Like in Figure 1, the cantilever can be stable only in an upper bending or lower bending position due to repulsive force between magnets. The

nominal equilibrium will lose stability, and new stable equilibrium positions will appear at a particular distance between two magnets. Figure 9 shows the voltage vs. frequency plots for different grading indexes and distances between the magnets. From Figure 9, we can conclude that energy harvesters can act as linear harvesters or nonlinear harvesters, depending on the distance between the magnets. For higher values of d_0, the energy harvester is a linear harvester, because the force due to the magnets is small. However, as two magnets come closer, the generated repulsive magnetic force increases, which changes the linear harvester into a nonlinear harvester. In this study, for a distance $d_0 = 0.4$ mm, the magnetic force is higher, due to which the system is bistable as shown in Figure 9a. A second observation from Figure 9a is that as the grading index (n) increases, the nonlinearity of the harvester increases and reduces the voltage output. For different grading index values (n), the harvester responses are quite different for a fixed magnetic distance due to the change in stiffness of the harvesters. The voltage peak is a maximum for $n = 0$ while it is a minimum for $n = 1000$. A change in voltage is observed due the change in the material characteristics of the harvester. We can conclude that the electric performance decreases while the mechanical performance increases at layer interfaces by increasing the grading index value (n). As the distance between magnets increases, the nonlinear effect decreases and moves towards the linear behavior as shown in Figure 9b–f. For distance $d_0 = 1$ mm and $d_0 = 10$ mm, the voltage plots are almost similar, which indicates that there is a negligible effect of magnetic force, and linear behavior of the harvester is observed.
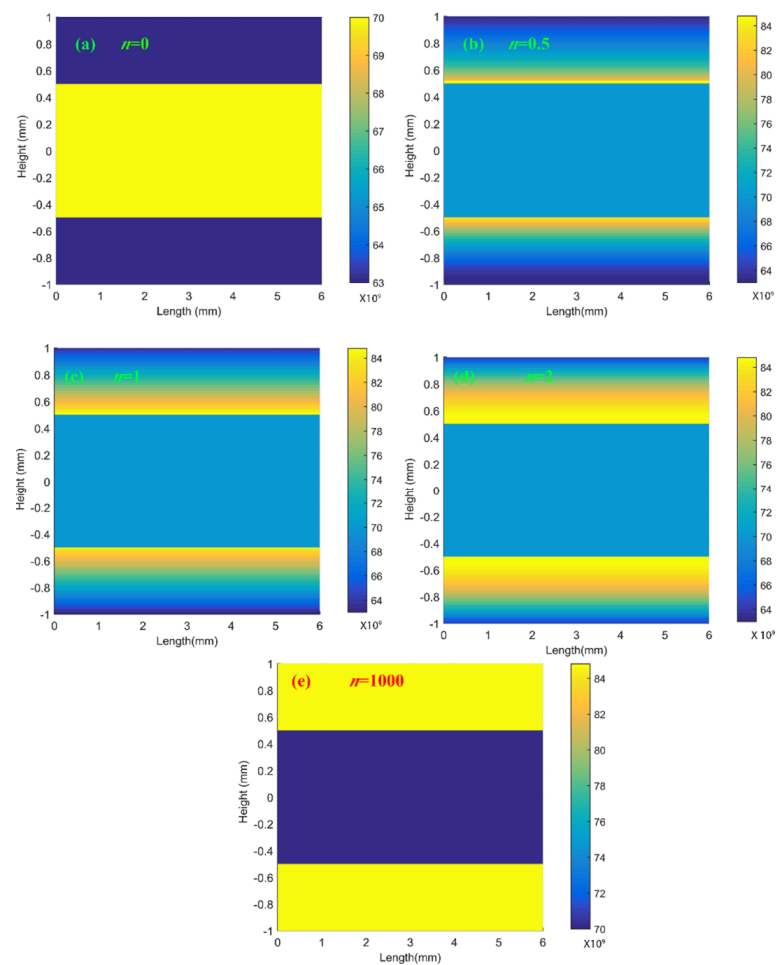

Figure 7. Young's modulus variation along the thickness of the piezoelectric material and host structure for different grading indexes (**a**) $n = 0$, (**b**) $n = 0.5$, (**c**) $n = 1$, (**d**) $n = 2$ and (**e**) $n = 1000$.
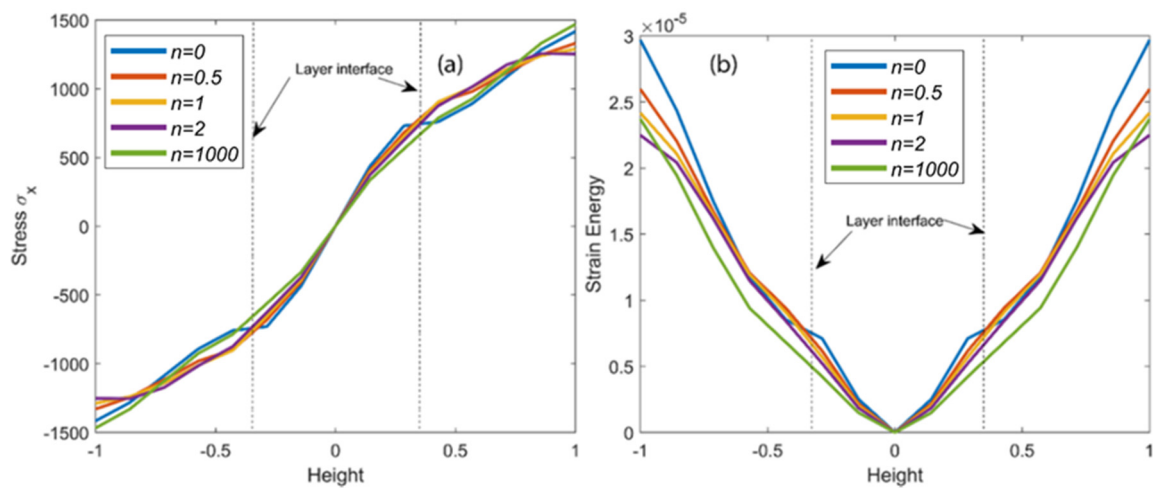
Figure 8. (**a**) Stress and (**b**) strain energy variations in thickness direction of the energy harvester for different grading indexes (*n*).

However, for an energy harvesting application, the voltage is not a clear indicator of the performance of the harvester. The power across the load resistance (R) is an important output parameter of the energy harvester, which can be calculated using Equation (6). To harvest the maximum energy, it is required to use optimum resistance across the piezoelectric material. However, in the case of piezoelectric energy harvesting, optimum resistance can be written as $1/\omega c_p$, which is equal to the impedance of the piezoelectric layer [26]. Figure 10 shows the power output vs. frequency for different grading indexes and magnetic distance. Patterns of the graphs are similar to the voltage. As the distance (d_0) increases, the nonlinear effect in the structure reduces. By decreasing the nonlinear effect, the peak of the power output increases while the effective harvesting frequency bandwidth decreases for each grading index. For example, at d_0 = 0.4 mm and *n* = 1, the effecting harvesting frequency range is 20 Hz to 85 Hz, while at d_0 = 10 mm the effective harvesting frequency range is 35 Hz to 65 Hz. There is an approximately 216% increase of effective harvesting frequency bandwidth at a distance of 0.4 mm as compared to the bandwidth at a distance of d_0 = 10 mm. The peak voltage and power out of a nonlinear energy harvester at different magnetic distances and grading indexes have been summarize in Table 5.

In this study we further extend the simulations in a time domain. For time domain simulations, we fix the excitation frequency to 5 Hz, which is far away from its natural frequency (about 51 Hz), for each grading index and compare the voltage output for the bistable and linear harvester. Obtained results are plotted in Figure 11. Figure 11a,c,e,g,i are plotted for velocity vs. amplitude, and Figure 11b,d,f,h,j are plotted for voltage vs. time at different distances between the magnets. From the figure it can be observed that for the nonlinear harvester the velocity and voltage output are much higher as compared to the linear harvester. Velocity vs. displacement plots verify the bistability of the harvester for a nonlinear behavior of the harvester, while the second plot shows the voltage comparison for linear and bistable harvesters. As the grading index (*n*) increases the output, voltage decreases, which confirms that at a higher grading index the electric performance of the harvester decreases. From the Figure 11, we can conclude that the nonlinear harvester is much more effective than the linear harvester, for excitation frequencies away from its resonance frequency.
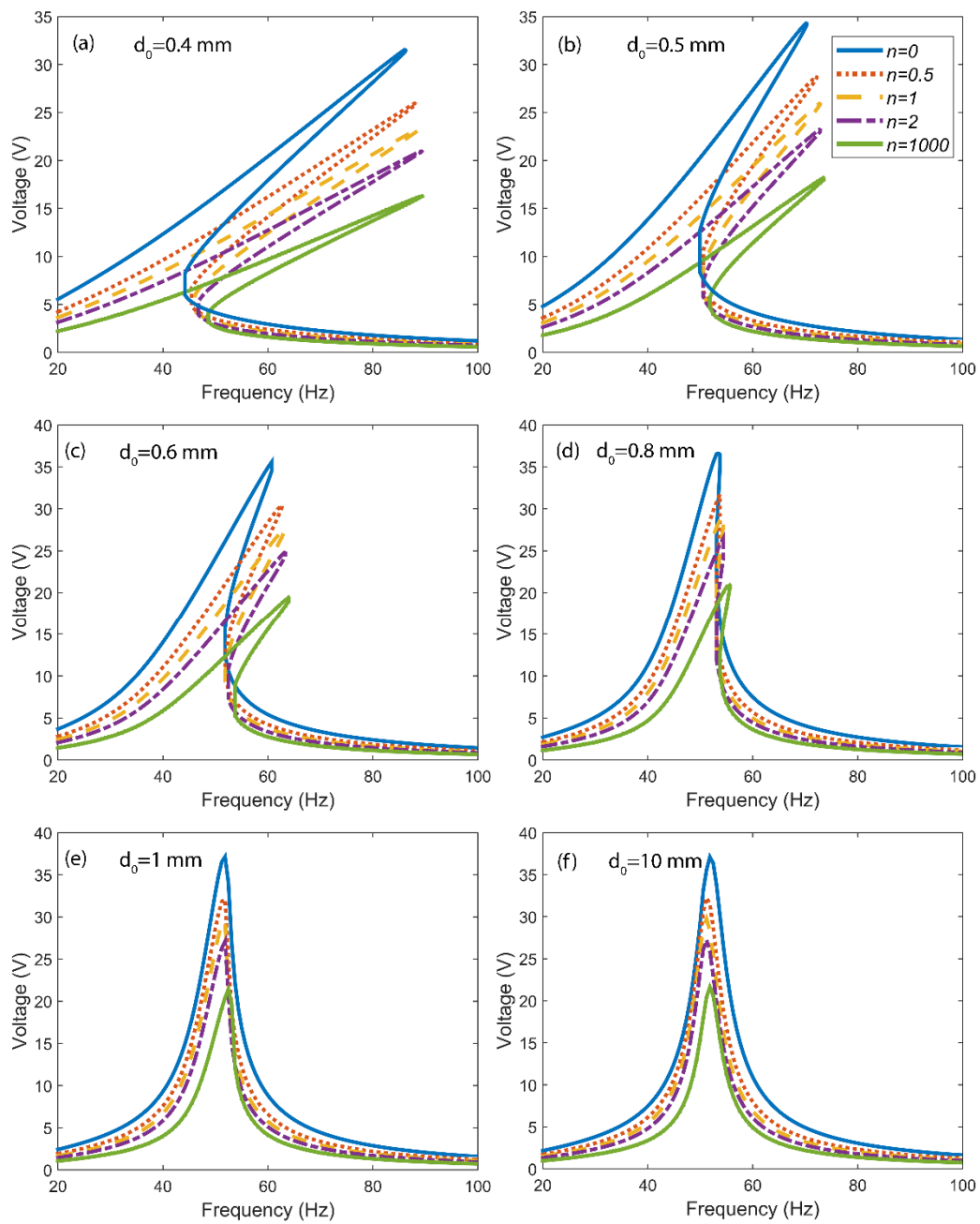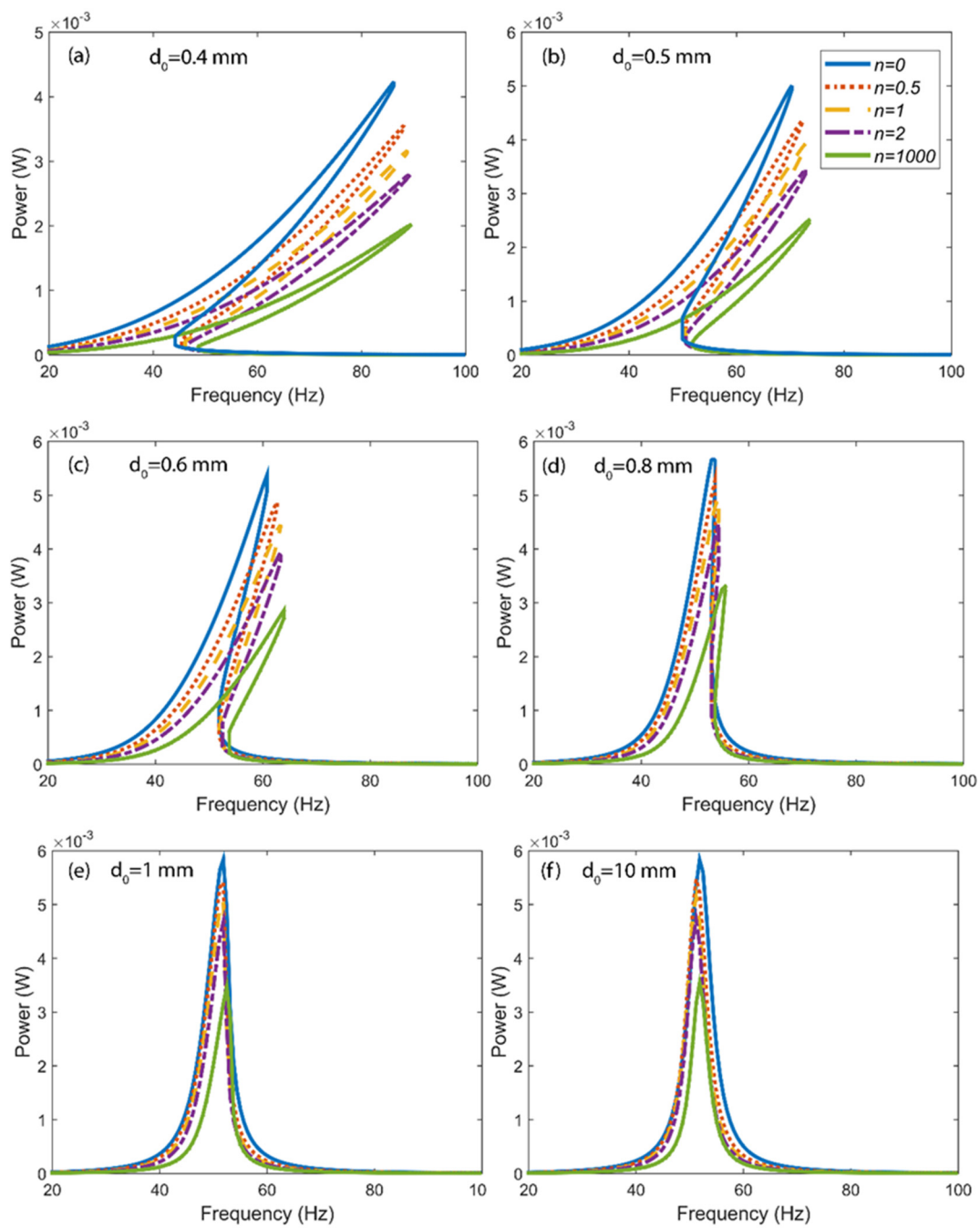
Figure 9. Voltage responses of an FGPM nonlinear energy harvester for different magnetic distances (d_0) and grading indexes at (**a**) $d_0 = 0.4$ mm (**b**) $d_0 = 0.5$ mm (**c**) $d_0 = 0.6$ mm (**d**) $d_0 = 0.8$ mm (**e**) $d_0 = 1$ mm (**f**) $d_0 = 10$ mm.

Figure 10. Power responses of a FGPM nonlinear energy harvester for different magnetic distances (d_0) and grading indexes at (**a**) d_0 = 0.4 mm (**b**) d_0 = 0.5 mm (**c**) d_0 = 0.6 mm (**d**) d_0 = 0.8 mm (**e**) d_0 = 1 mm (**f**) d_0 = 10 mm.

Table 5. Summary of peak output voltage and power for nonlinear energy harvester.

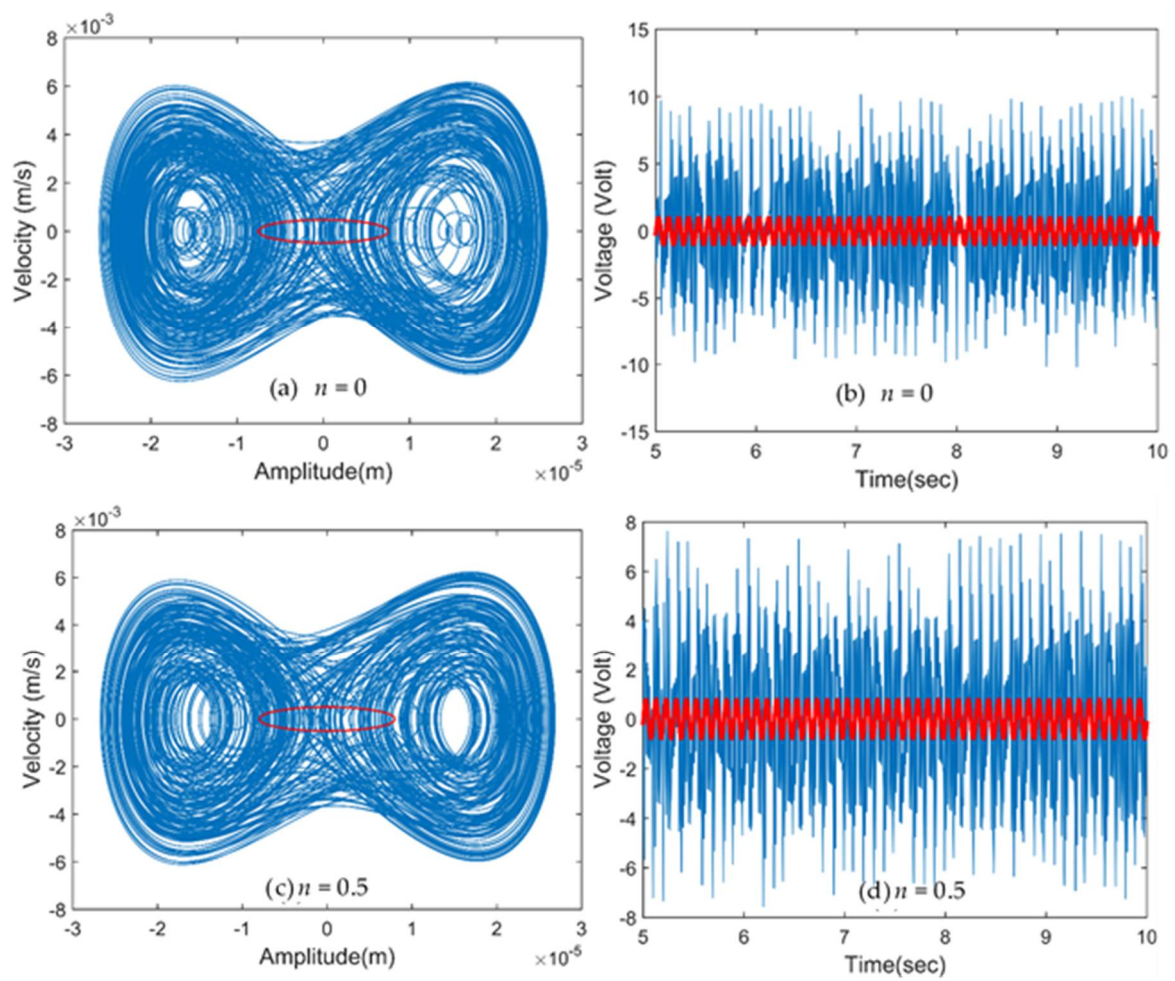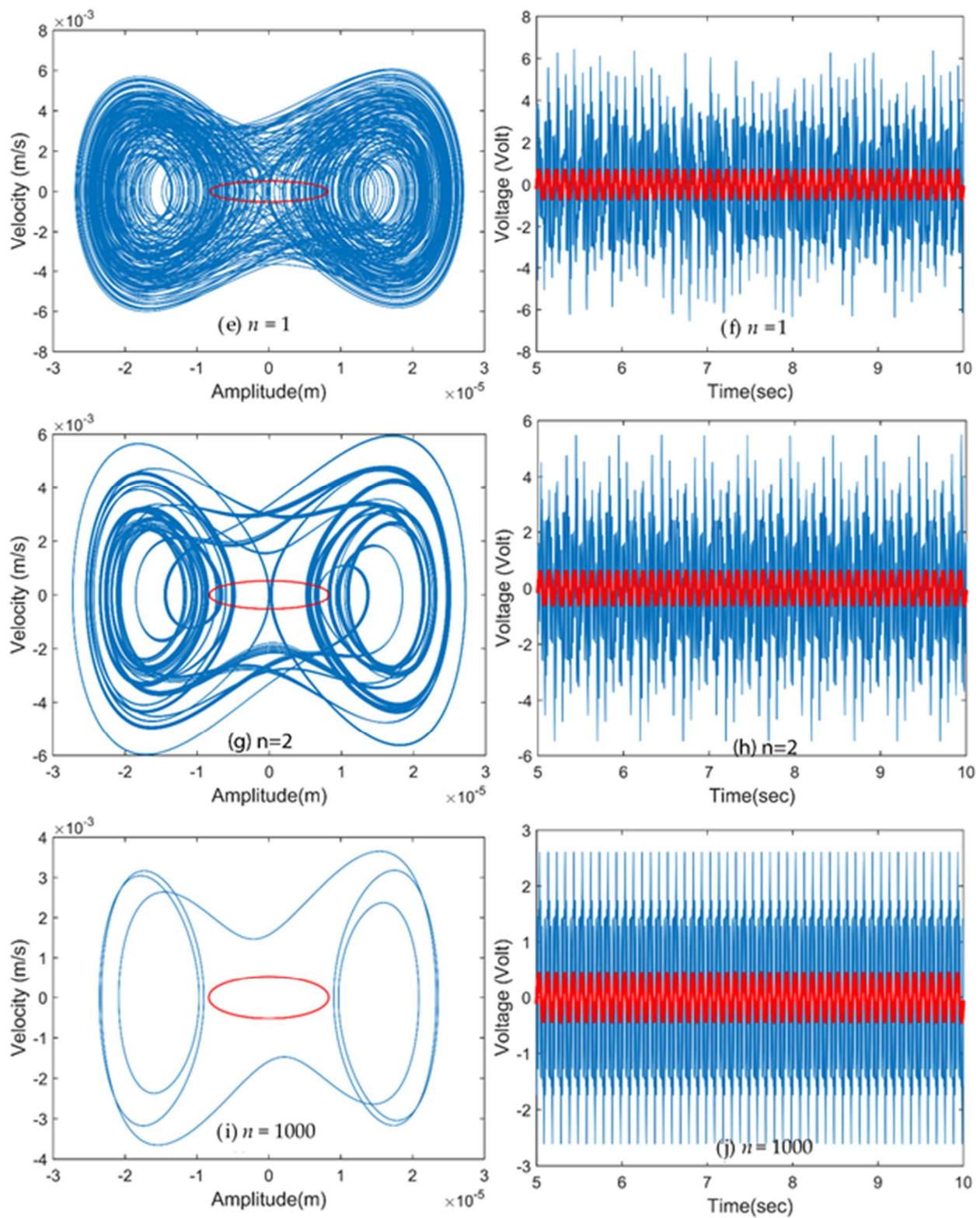| d_0 (mm)	n = 0		n = 0.5		n = 1		n = 2		n = 1000	
	Voltage (V)	Power (mW)	Voltage (V)	Power (mW)	Voltage (V)	Power (mW)	Voltage (V)	Power (mW)	Voltage (V)	Power (mW)
0.4	31.23	4.2	25.46	3.5	23.72	3.1	21.24	2.8	16.25	2.0
0.5	34.39	5.0	28.78	4.3	26	3.9	23.29	3.4	18.01	2.5
0.6	35.61	5.3	30.18	4.8	27.66	4.4	24.88	3.9	19.45	2.8
0.8	36.59	5.6	31.68	5.2	29.19	4.9	26.48	4.4	20.9	3.3
1	37.13	5.8	31.81	5.4	29.54	5.0	27.1	4.6	21.38	3.4
10	37.2	5.8	32.25	5.4	29.73	5.1	27.21	4.7	21.62	3.5

Figure 11. *Cont.*

Figure 11. Time domain response of a bistable energy harvester and linear energy harvester for force excitation frequency (f = 5 Hz) for each grading index and d_0 = 0.4 mm (▬ Linear harvester, ▬ Non Linear harvester). (**a,b**) at n = 0; (**c,d**) at n = 0.5; (**e,f**) at n = 1; (**g,h**) at n = 2; (**i,j**) at n = 1000.

5. Conclusions

In the present approach, we have converted a multi-degree system into single-degree system to solve with a harmonic balance method. Mechanical system equations are coupled with an electric equation due to piezoelectric constitutive equations. The distance between magnets also has a great impact on the solution of coupled equations. Energy harvesting using functionally graded piezoelectric material has been explored using the finite element method for a linear and a nonlinear energy harvester. Non-linearity has been introduced using two magnets that represent a Duffing's oscillator. The simple harmonic balance method has been employed to obtain the harvester response in a frequency domain. In addition, voltage and power responses have also been computed in a time domain. It is established that as the distance between magnets decreases, the degree of non-linearity between the system increases, and the effective working frequency bandwidth also increases significantly. The effective harvesting frequency range for $d_0 = 0.4$ mm and $n = 1$ is observed to be 20 Hz to 85 Hz, while it was only between 35 Hz to 65 Hz for $d_0 = 10$ mm, therefore yielding a 216% increase in the frequency bandwidth. By introducing functional grading in piezoelectric layers, a smooth stress variation is ensured at the layer interfaces, minimizing the possibility of debonding. However, a decrease in power output is recorded with grading in material properties. The decrease in electrical performance varies with the magnetic distance and the value of grading index; e.g., a decrease of 10% to 50% is seen for $n = 0.5$ to 1000, for a value of $d_0 = 0.4$ mm, while for $d_0 = 1$ mm this decrease ranges from 12% to 28% for $n = 0.5$ to 1000. Under different case studies, the peak output power varied from 2 mW ($d_0 = 0.4$ mm and $n = \infty$) to 6 mW ($d_0 = 10$ mm and $n = 0$). It is true the power decreases with increasing the ratio of PZT-20%PT to PZT-0%PT, but it also decreases the delamination at the layers interface. This is also an important factor to consider, the life of the energy harvester system, as these systems are potential substitutes for batteries. Based on the application and nature of vibration, the right selection can be done based on the grading index and distance between magnets (degree of nonlinear system in the harvester). In the present study, we focused on energy harvesting using functionally graded piezoelectric material. This study highlights the selection of a harvester parameter based on working conditions and applications. For example, a linear harvester is good where the exciting frequency is not much varying, and there is less possibility of the delamination of the piezoelectric layer. However, if there is a possibility of the delamination of layers due to environmental conditions, then the selection of the linear harvester is not good. In the energy harvester, delamination can occur between the piezoelectric and host layers due to the mechanical properties difference at the contact surface. Due to their difference in properties, both layers behave differently at the contact source. For example, if there is a change in operating temperature frequently, delamination can be possible due to a thermal expansion difference. Based on the working condition, parameters of the harvester can be optimized using a grading index and degree of nonlinearity in the system.

Data Availability Statement: Not applicable.

Conflicts of Interest: The authors declare no conflict of interest.

References

1. Arrieta, A.F.; Hagedorn, P.; Erturk, A.; Inman, D.J. A piezoelectric bistable plate for nonlinear broadband energy harvesting. *Appl. Phys. Lett.* **2010**, *97*, 104102. [CrossRef]
2. Challa, V.R.; Prasad, M.G.; Shi, Y.; Fisher, F.T. A vibration energy harvesting device with bidirectional resonance frequency tunability. *Smart Mater. Struct.* **2008**, *17*, 015035. [CrossRef]
3. Iliuk, I.; Brasil, R.M.L.R.D.F.; Balthazar, J.M.; Tusset, A.M.; Piccirillo, V.; Piqueira, J.R.C. Potential Application in Energy Harvesting of Intermodal Energy Exchange in a Frame: FEM Analysis. *Int. J. Struct. Stab. Dyn.* **2014**, *14*, 1440027. [CrossRef]
4. Mann, B.; Owens, B. Investigations of a nonlinear energy harvester with a bistable potential well. *J. Sound Vib.* **2010**, *329*, 1215–1226. [CrossRef]
5. Zhu, D.; Tudor, M.J.; Beeby, S. Strategies for increasing the operating frequency range of vibration energy harvesters: A review. *Meas. Sci. Technol.* **2009**, *21*, 22001. [CrossRef]
6. Mann, B.; Sims, N. Energy harvesting from the nonlinear oscillations of magnetic levitation. *J. Sound Vib.* **2009**, *319*, 515–530. [CrossRef]
7. Ramlan, R.; Brennan, M.J.; Mace, B.R.; Kovacic, I. Potential benefits of a non-linear stiffness in an energy harvesting device. *Nonlinear Dyn.* **2010**, *59*, 545–558. [CrossRef]
8. Daqaq, M.F. Response of uni-modal duffing-type harvesters to random forced excitations. *J. Sound Vib.* **2010**, *329*, 3621–3631. [CrossRef]
9. Stanton, S.C.; Erturk, A.; Mann, B.; Inman, D.J. Nonlinear piezoelectricity in electroelastic energy harvesters: Modeling and experimental identification. *J. Appl. Phys.* **2010**, *108*, 074903. [CrossRef]
10. Fan, K.-Q.; Chao, F.-B.; Zhang, J.-G.; Wang, W.-D.; Che, X.-H. Design and experimental verification of a bi-directional nonlinear piezoelectric energy harvester. *Energy Convers. Manag.* **2014**, *86*, 561–567. [CrossRef]
11. Qiu, J.; Tani, J.; Ueno, T.; Morita, T.; Takahashi, H.; Du, H. Fabrication and high durability of functionally graded piezoelectric bending actuators. *Smart Mater. Struct.* **2003**, *12*, 115–121. [CrossRef]
12. Chen, W.Q.; Ding, H.J. On free vibration of a functionally graded piezoelectric rectangular plate. *Acta Mech.* **2002**, *153*, 207–216. [CrossRef]
13. Yang, J.; Xiang, H. Thermo-electro-mechanical characteristics of functionally graded piezoelectric actuators. *Smart Mater. Struct.* **2007**, *16*, 784–797. [CrossRef]
14. Li, C.; Weng, G. Antiplane crack problem in functionally graded piezoelectric materials. *J. Appl. Mech.* **2002**, *69*, 481–488. [CrossRef]
15. Rajasekaran, S. Free vibration of centrifugally stiffened axially functionally graded tapered Timoshenko beams using differential transformation and quadrature methods. *Appl. Math. Model.* **2013**, *37*, 4440–4463. [CrossRef]
16. Takagi, K.; Li, J.-F.; Yokoyama, S.; Watanabe, R. Fabrication and evaluation of PZT/Pt piezoelectric composites and functionally graded actuators. *J. Eur. Ceram. Soc.* **2003**, *23*, 1577–1583. [CrossRef]
17. Rafiee, M.; He, X.Q.; Liew, K.M. Nonlinear analysis of piezoelectric nanocomposite energy harvesting plates. *Smart Mater. Struct.* **2014**, *23*, 65001. [CrossRef]
18. Amini, Y.; Fatehi, P.; Heshmati, M.; Parandvar, H. Time domain and frequency domain analysis of functionally graded piezoelectric harvesters subjected to random vibration: Finite element modeling. *Compos. Struct.* **2016**, *136*, 384–393. [CrossRef]
19. Ng, T.Y.; He, X.; Liew, K.M. Finite element modeling of active control of functionally graded shells in frequency domain via piezoelectric sensors and actuators. *Comput. Mech.* **2002**, *28*, 1–9. [CrossRef]
20. Amini, Y.; Emdad, H.; Farid, M. Finite element modeling of functionally graded piezoelectric harvesters. *Compos. Struct.* **2015**, *129*, 165–176. [CrossRef]
21. Pradyumna, S.; Bandyopadhyay, J. Free vibration analysis of functionally graded curved panels using a higher-order finite element formulation. *J. Sound Vib.* **2008**, *318*, 176–192. [CrossRef]
22. Susheel, C.K.; Kumar, R.; Chauhan, V.S. Active shape and vibration control of functionally graded thin plate using functionally graded piezoelectric material. *J. Intell. Mater. Syst. Struct.* **2016**, *28*, 1789–1802. [CrossRef]
23. Kumar, T.; Kumar, R.; Chauhan, V.S.; Twiefel, J. Finite-Element Analysis of a Varying-Width Bistable Piezoelectric Energy Harvester. *Energy Technol.* **2015**, *3*, 1243–1249. [CrossRef]
24. Xie, Z.; Kwuimy, C.A.K.; Wang, T.; Ding, X.; Huang, W. Theoretical analysis of an impact-bistable piezoelectric energy harvester. *Eur. Phys. J. Plus* **2019**, *134*, 190. [CrossRef]
25. Erturk, A.; Inman, D.J. An experimentally validated bimorph cantilever model for piezoelectric energy harvesting from base excitations. *Smart Mater. Struct.* **2009**, *18*, 025009. [CrossRef]
26. Sebald, G.; Kuwano, H.; Guyomar, D.; Ducharne, B. Experimental Duffing oscillator for broadband piezoelectric energy harvesting. *Smart Mater. Struct.* **2011**, *20*, 102001. [CrossRef]
27. Stanton, S.C.; Owens, B.A.; Mann, B.P. Harmonic balance analysis of the bistable piezoelectric inertial generator. *J. Sound Vib.* **2012**, *331*, 3617–3627. [CrossRef]

28. Al-Ashtari, W.; Hunstig, M.; Hemsel, T.; Sextro, W. Frequency tuning of piezoelectric energy harvesters by magnetic force. *Smart Mater. Struct.* **2012**, *21*, 035019. [CrossRef]

29. Marathe, A.; Govindarajan, R. Nonlinear Dynamical Systems, Their Stability, and Chaos Lecture notes from the FLOW-NORDITA Summer School on Advanced Instability Methods for Complex Flows, Stockholm, Sweden, 2013. *Appl. Mech. Rev.* **2014**, *66*, 24802. [CrossRef]